

Fault-Tolerant Control for Electric Ground Vehicles With Independently-Actuated In-Wheel Motors

Rongrong Wang

e-mail: wang.1862@osu.edu

Junmin Wang¹

e-mail: wang.1381@osu.edu

Department of Mechanical and Aerospace
Engineering,
The Ohio State University,
Columbus, OH 43210

This paper presents an in-wheel motor fault diagnosis and fault-tolerant control method for four-wheel independently actuated (4WIA) electric vehicles. The 4WIA electric vehicle is one of the promising architectures for electric vehicles. While such a vehicle architecture greatly increases the flexibility for vehicle control, it also elevates the requirements on system reliability, safety, and fault tolerance due to the increased number of actuators. A fault diagnosis approach for finding the faulty in-wheel motor/motor driver pair is developed. The proposed diagnosis approach does not need an accurate knowledge on tire-road friction coefficient (TRFC) and is robust to tire force modeling inaccuracies. Based on the in-wheel motor/motor driver fault diagnosis mechanism, a control-allocation based vehicle fault-tolerant control system is designed to accommodate the in-wheel motor/motor driver fault by automatically allocating the control effort among other healthy wheels. Simulations using a high-fidelity, CarSim®, full-vehicle model show the effectiveness of the proposed in-wheel motor/motor driver fault diagnosis and fault-tolerant control approaches. [DOI: 10.1115/1.4005050]

Keywords: control, fault-tolerant, in-wheel motor, electric vehicle

1 Introduction

Hybrid electric, plug-in hybrid electric, and pure electric vehicles have been considered as promising vehicle architectures due to their remarkable potentials in emissions and fuel consumption reductions [1,2]. Among these vehicle architectures, the four-wheel independently actuated (4WIA) electric vehicle is an emerging one. The 4WIA electric vehicles employ four in-wheel (or hub) motors to drive the four wheels, respectively. The torque and driving/braking mode of each wheel can be controlled independently. Such actuation flexibility together with the electric motors' fast and precise torque responses may enhance the existing vehicle control strategies, e.g., traction control system and direct yaw-moment control, and other advanced vehicle motion/stability control methods [3–7]. However, in comparison to the conventional vehicle architectures, the probability for a fault, e.g., in-wheel motor fault, takes place in a 4WIA electric vehicle is higher primarily due to the significantly increased system complexity and number of actuators. The in-wheel motor faults may be caused by mechanical failures, overheat of the motors, or faults associated with the motor drivers. When such a fault occurs, the faulty wheel may fail to provide the expected torque and thus jeopardize the vehicle motion control [8]. Without appropriate controls/accommodations, the in-wheel motor or motor driver faults may result in an unsatisfactory performance or even instability for the 4WIA electric vehicles. Therefore, the demands on reliability, safety, and fault tolerance for the 4WIA electric vehicles are substantially elevated. It is thus necessary to design control systems which are capable of detecting, identifying, and tolerating potential in-wheel motor faults, in order to improve the reliability while maintaining desirable stability and performance of such vehicles. Several fault diagnosis and fault-tolerant control strategies for

ground vehicles have been previously suggested in the literature [9–11]. However, most of these algorithms dealt with the problems associated with conventional vehicle architectures, but not for the 4WIA electric vehicles. Several fault diagnosis and fault-tolerant control methods for electric motors were also proposed and reviewed in Refs. [12, 13]. However, certain motor faults, such as the bearing fault, are difficult to diagnose only with the current and voltage sensors [13]. An alternative way of doing the in-wheel motor diagnosis for 4WIA electric vehicles is proposed in this paper. This method potentially can be combined with other existing motor fault diagnosis methods to decrease the chance of misdiagnosis and improve the system robustness.

This paper considers the in-wheel motor/motor driver fault diagnosis and fault-tolerant control for the 4WIA electric vehicles. A fault diagnosis approach to locate the faulty in-wheel/motor driver pair is proposed. Based on the diagnosis information, a fault accommodating control approach is then designed to maintain the desired vehicle motion. As the tire-road friction coefficient (TRFC) is generally unknown, the proposed fault diagnosis approach is developed with a TRFC on-line estimator. The robustness of the fault diagnosis approach is also studied, and it is shown that the diagnosis approach can work well in the presence of disturbances and tire modeling errors. To improve the system robustness against some possible unmodeled dynamics and disturbances, a sliding mode controller (SMC) in conjunction with a control allocation scheme were used to design a fault-tolerant controller (FTC) to accommodate the in-wheel motor/motor driver fault. Due to the measurement noise, directly using the time derivative of wheel angular speed signal may be challenging, an estimator is thus proposed to obtain this signal. Simulations using a high-fidelity CarSim® vehicle model illustrate the effectiveness of the proposed strategies in different driving scenarios.

The rest of the paper is organized as follows. System modeling is presented in Sec. 2. In-wheel motor/motor driver pair fault diagnosis method design is described in Sec. 3. The 4WIA electric vehicle fault-tolerant control method is described in Sec. 4. Simulation results are presented in Sec. 5 followed by conclusive remarks.

¹Corresponding author.

Contributed by the Dynamic Systems Division of ASME for publication in the JOURNAL OF DYNAMIC SYSTEMS, MEASUREMENT, AND CONTROL. Manuscript received August 3, 2010; final manuscript received July 25, 2011; published online January 11, 2012. Assoc. Editor: Douglas Adams.

2 System Modeling and Problem Formulation

2.1 Vehicle Model. A schematic diagram of a vehicle model is shown in Fig. 1. Ignoring the pitch and roll motion, the vehicle has three degrees of freedom for longitudinal motion, lateral motion, and yaw motion. Vehicle equations of motion in longitudinal, lateral, and yaw directions can be expressed as follows [14,15]:

$$\begin{cases} \dot{V}_x = V_y \Omega_z - \frac{C_d}{M} V_x^2 + \frac{1}{M} F_X \\ \dot{V}_y = -V_x \Omega_z + \frac{1}{M} F_Y \\ \dot{\Omega}_z = \frac{1}{I_z} M_z \end{cases} \quad (1)$$

where V_x and V_y are longitudinal speed and lateral speed, respectively, Ω_z is the yaw rate. M is the mass of the vehicle, and I_z is the yaw inertia, and C_d is the aerodynamic drag term. F_X , F_Y , and M_z are the total forces/moment represented by the summation of the tire forces generated at all the four tires, and can be defined by

$$\begin{cases} F_X = (F_{xfl} + F_{xfr}) \cos \sigma - (F_{yfl} + F_{yfr}) \sin \sigma + F_{xrl} + F_{xrr} \\ F_Y = (F_{yfl} + F_{yfr}) \cos \sigma + (F_{xfl} + F_{xfr}) \sin \sigma + F_{yrl} + F_{yrr} \\ M_z = (F_{yfl} \sin \sigma - F_{xfl} \cos \sigma - F_{xrl} + F_{xrr} + F_{xfr} \cos \sigma - F_{yfr} \sin \sigma) l_s \\ \quad - (F_{yfr} + F_{yrr}) l_r + ((F_{yfr} + F_{xfl}) \cos \sigma + (F_{xfr} + F_{xfl}) \sin \sigma) l_f \end{cases} \quad (2)$$

where, σ is the road wheel angle of the front wheels. Based on Eq. (2), rewrite Eq. (1) as

$$\begin{bmatrix} \dot{V}_x \\ \dot{V}_y \\ \dot{\Omega}_z \end{bmatrix} = \begin{bmatrix} V_y \Omega_z - \frac{C_d}{M} V_x^2 \\ -V_x \Omega_z \\ 0 \end{bmatrix} + B_y F_y + B_x F_x \quad (3)$$

where $F_x = [F_{xfl} \ F_{xfr} \ F_{xrl} \ F_{xrr}]^T$, $F_y = [F_{yfl} \ F_{yfr} \ F_{yrl} \ F_{yrr}]^T$, and

$$B_x = \begin{bmatrix} \frac{1}{M} & 0 & 0 \\ 0 & \frac{1}{M} & 0 \\ 0 & 0 & \frac{1}{I_z} \end{bmatrix} \begin{bmatrix} \cos \sigma & \cos \sigma & 1 & 1 \\ \sin \sigma & \sin \sigma & 0 & 0 \\ l_f \sin \sigma - l_s \cos \sigma & l_f \sin \sigma + l_s \cos \sigma & -l_s & l_s \end{bmatrix}$$

$$B_y = \begin{bmatrix} \frac{1}{M} & 0 & 0 \\ 0 & \frac{1}{M} & 0 \\ 0 & 0 & \frac{1}{I_z} \end{bmatrix} \begin{bmatrix} -\sin \sigma & -\sin \sigma & 0 & 0 \\ \cos \sigma & \cos \sigma & 1 & 1 \\ l_f \cos \sigma + l_s \sin \sigma & l_f \cos \sigma - l_s \sin \sigma & -l_r & -l_r \end{bmatrix}$$

In this study, each pair of in-wheel motor and its driver is treated as a unit. The mechanical motion of a motor is much slower than

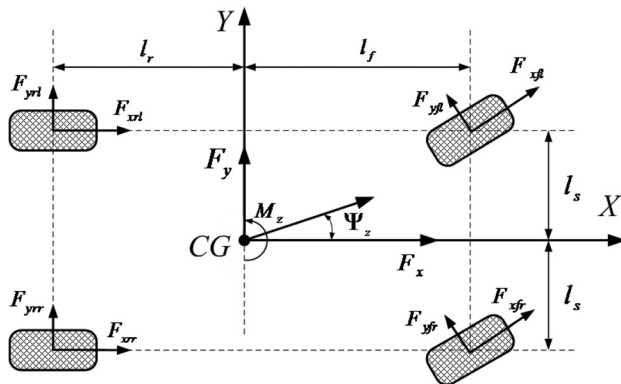


Fig. 1 Schematic diagram of a vehicle model

the electromagnetic dynamics, implying that the dynamic response of the motor driver and in-wheel motor can be ignored. So the motor driver and in-wheel motor pair model can be represented by a control gain k_i , which is defined as

$$k_i = \frac{T_i}{u_i} \quad (4)$$

where $i \in Q := \{fl, fr, rl, rr\}$ indicates the specific tire, T_i is the output torque of the in-wheel motor, u_i is the torque control signal to the motor's driver. This control gain value will be used as a reference for the diagnosis purpose.

The tire longitudinal forces can be calculated based on the wheels' rotational dynamics, and can be represented by

$$F_x = \begin{bmatrix} F_{xfl} \\ F_{xfr} \\ F_{xrl} \\ F_{xrr} \end{bmatrix} = \frac{1}{R_{\text{eff}}} \begin{bmatrix} k_{fl} & 0 & 0 & 0 \\ 0 & k_{fr} & 0 & 0 \\ 0 & 0 & k_{rl} & 0 \\ 0 & 0 & 0 & k_{rr} \end{bmatrix} \begin{bmatrix} u_{fl} \\ u_{fr} \\ u_{rl} \\ u_{rr} \end{bmatrix} - \frac{1}{R_{\text{eff}}} \begin{bmatrix} I_{\omega} \dot{\omega}_{fl} \\ I_{\omega} \dot{\omega}_{fr} \\ I_{\omega} \dot{\omega}_{rl} \\ I_{\omega} \dot{\omega}_{rr} \end{bmatrix} - \begin{bmatrix} F_{fl_roll} \\ F_{fr_roll} \\ F_{rl_roll} \\ F_{rr_roll} \end{bmatrix} \quad (5)$$

where ω_i is the tire longitudinal rotational speed in rad/s, R_{eff} is the tire effective rolling radius in meter, F_{i_roll} is the i th tire rolling resistance. Thus, based on Eq. (5), the vehicle model Eq. (3) can be written as

$$\dot{X} = f(X) + BU \quad (6)$$

with,

$$X = \begin{bmatrix} V_x \\ V_y \\ \Omega_z \end{bmatrix},$$

$$f(X) = \begin{bmatrix} V_y \Omega_z - \frac{C_d}{M} V_x^2 \\ -V_x \Omega_z \\ 0 \end{bmatrix} + B_y F_y - \frac{B_x}{R_{\text{eff}}} \begin{bmatrix} I_{\omega} \dot{\omega}_{fl} \\ I_{\omega} \dot{\omega}_{fr} \\ I_{\omega} \dot{\omega}_{rl} \\ I_{\omega} \dot{\omega}_{rr} \end{bmatrix}, \quad -B_x \begin{bmatrix} F_{fl_roll} \\ F_{fr_roll} \\ F_{rl_roll} \\ F_{rr_roll} \end{bmatrix},$$

$$B = \frac{B_x}{R_{\text{eff}}} \begin{bmatrix} k_{fl} & 0 & 0 & 0 \\ 0 & k_{fr} & 0 & 0 \\ 0 & 0 & k_{rl} & 0 \\ 0 & 0 & 0 & k_{rr} \end{bmatrix}, \quad U = \begin{bmatrix} u_{fl} \\ u_{fr} \\ u_{rl} \\ u_{rr} \end{bmatrix}$$

From the above vehicle motion and tire force models, it can be seen that when one of the four in-wheel motors or one of the four motor drivers has a fault, without respective accommodating control action, the vehicle may rapidly deviate from the expected trajectory as the torque provided by the faulty wheel will be less than expected.

The slip angle of each tire can be defined as the angular difference between the orientation of a wheel and the velocity of the wheel center

$$\begin{cases} \alpha_{fl} = -\sigma + \tan^{-1} \left(\frac{V_y + \Omega_z l_f}{V_x - \Omega_z l_s} \right) \\ \alpha_{fr} = -\sigma + \tan^{-1} \left(\frac{V_y + \Omega_z l_f}{V_x + \Omega_z l_s} \right) \\ \alpha_{rl} = \tan^{-1} \left(\frac{V_y - \Omega_z l_f}{V_x - \Omega_z l_s} \right) \\ \alpha_{rr} = \tan^{-1} \left(\frac{V_y - \Omega_z l_f}{V_x + \Omega_z l_s} \right) \end{cases} \quad (7)$$

The speeds at the wheel centers are

$$\begin{cases} V_{xfl} = (V_x - \Omega_z l_s) \cos \sigma + (V_y + \Omega_z l_f) \sin \sigma \\ V_{xfr} = (V_x + \Omega_z l_s) \cos \sigma + (V_y + \Omega_z l_f) \sin \sigma \\ V_{xrl} = V_x - \Omega_z l_s \\ V_{xrr} = V_x + \Omega_z l_s \end{cases} \quad (8)$$

The tire longitudinal slip ratio is defined as the relative difference between tire circumferential speed and tire center speed

$$s_i = \frac{\omega_i R_{\text{eff}} - V_{xi}}{\max(V_{xi}, \omega_i R_{\text{eff}})} \quad (9)$$

Based on advanced sensing such as global positioning system and inertia measurement unit, the vehicle yaw rate, longitudinal and lateral speeds can be measured [16], slip ratio, slip angle of each wheel, and the speed at the center of each tire can also be calculated [15]. In this paper, it is assumed that these advanced sensing systems can provide accurate measurements on such variables. Note that when a fault happens to an in-wheel motor or a motor driver, the estimation of the control gain of the motor/motor driver pair, \hat{k}_i , will be used in the B matrix.

2.2 Tire Model. One of the most well-known tire models is Pacejka's Magic Formula tire model [14,17]. The Magic Formula tire model is capable of producing characteristics that closely match measured curves for the tire lateral force F_y , longitudinal force F_x , and aligning moment as functions of slip angle α_i , and longitudinal slip ratio s_i . It has been widely used for vehicle dynamics simulations and analyses. The basic model equations are [14,17]

$$\begin{cases} y(x) = D \sin\{C \tan^{-1}[Bx - E(Bx - \tan^{-1} Bx)]\} \\ Y(X) = y(x) + S_v \\ x = X + S_h \end{cases} \quad (10)$$

where $Y(X)$ represents the tire longitudinal force, lateral force, or self-aligning moment, X is the tire slip or slip angle. Coefficient B is the stiffness factor, C is the shape factor, D is the peak factor, and E is the curvature factor. S_h and S_v denote the horizontal shift and vertical shift, respectively. These coefficients can be tuned to fit with experimental data for a given tire on a test patch. Figure 2 shows the normalized tire longitudinal force versus slip at different TRFCs, when the tire slip angle is zero. Note that the normalized longitudinal force increases with increase of the TRFC at given longitudinal slip ratio s_i and tire slip angle α_i . This characteristic will be used in the fault diagnosis design.

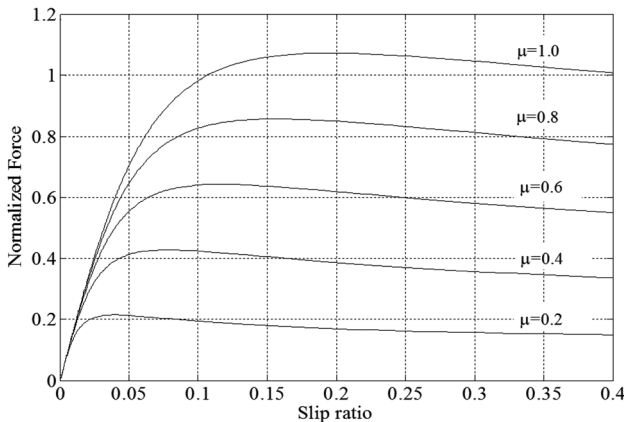


Fig. 2 Normalized tire longitudinal force versus slip ratios at different TRFCs

3 Fault Diagnosis Design

3.1 Fault Diagnosis Design Without Considering Modeling Errors. The rotational dynamics of each wheel during driving is represented by

$$I_\omega \dot{\omega}_i = k_i u_i - R_{\text{eff}}(F_{ix} + F_{i\text{-roll}}) \quad (11)$$

with the rolling resistance being described as

$$F_{i\text{-roll}} = F_{zi}(a + bV_{xi}^2) \quad (12)$$

where a is a coefficient in the order of 10^{-2} and b is a coefficient in the order of 10^{-8} . Typical passenger car tire rolling resistance coefficient is therefore very small and weakly depends on speed.

Due to the signal noise, wheel angular acceleration cannot be obtained by directly differentiating the measured wheel angular speed signal. Similar as the one presented in Ref. [18], thus an estimator is designed below

$$I_\omega \dot{\tilde{\omega}}_i = k_{0i} u_i - R_{\text{eff}}(\hat{F}_{ix} + \hat{F}_{i\text{-roll}}) + l\tilde{\omega}_i + \phi_i \quad (13)$$

where $l > 0$, k_{0i} is the known nominal motor control gain, $\tilde{\omega}_i = \omega_i - \hat{\omega}_i$, \hat{F}_{ix} and $\hat{F}_{i\text{-roll}}$ are tire longitudinal force and tire rolling resistance calculated based on the tire model. Based on Eqs. (11) and (13), one can have

$$\begin{aligned} I_\omega \dot{\tilde{\omega}}_i = & -l\tilde{\omega}_i + ((k_i - k_{0i})u_i + (\hat{F}_{ix} + \hat{F}_{i\text{-roll}} - F_{ix} - F_{i\text{-roll}}) \\ & \times R_{\text{eff}} - \phi_i) \end{aligned} \quad (14)$$

If the TRFC, tire model, and rolling resistance model are all accurate, the following will hold:

$$\hat{F}_{ix} + \hat{F}_{i\text{-roll}} - F_{ix} - F_{i\text{-roll}} = 0 \quad (15)$$

Thus, Eq. (14) can be written as

$$I_\omega \dot{\tilde{\omega}}_i = -l\tilde{\omega}_i + (k_i - k_{0i})u_i - \phi_i \quad (16)$$

When $k_i = k_{0i}$, there is no fault happens to the wheel, while $k_i \neq k_{0i}$ will indicate that a fault happens.

Choose the adaptation law for ϕ_i as

$$\dot{\phi}_i = \gamma \tilde{\omega}_i, \quad \gamma > 0 \quad (17)$$

Differentiating Eq. (16) can result in

$$I_\omega \ddot{\tilde{\omega}}_i + l\dot{\tilde{\omega}}_i + \gamma \tilde{\omega}_i = (k_i - k_{0i})\dot{u}_i \quad (18)$$

It can be seen that by choosing sufficiently large γ and l , $\tilde{\omega}_i$ and $\dot{\tilde{\omega}}_i$ will be arbitrarily small as long as \dot{u}_i is bounded. In normal driving scenarios, such as constant speed cruising, it is reasonable to assume that the change of u_i is small. So, one may have that $\tilde{\omega}_i$ and $\dot{\tilde{\omega}}_i$ will converge to 0 fast.

Based on Eq. (16), one has

$$\phi_i = (k_i - k_{0i})u_i - I_\omega \ddot{\tilde{\omega}}_i - l\dot{\tilde{\omega}}_i \quad (19)$$

After $\tilde{\omega}_i$ and $\dot{\tilde{\omega}}_i$ converge to 0, one can have $\phi_i = (k_i - k_{0i})u_i = 0$, if there is no fault happens. If $k_i \neq k_{0i}$, $\phi_i = (k_i - k_{0i})u_i \neq 0$. Thus, it can be concluded that if $\phi_i = 0$, there is no fault for the respective in-wheel motor/motor controller pair, and $\phi_i \neq 0$ indicates a fault. The control gain estimation in this case can be written as $\hat{k}_i = k_{0i} - \frac{\phi_i}{u_i}$.

However, in most cases, the TRFC is unknown, so ϕ_i cannot be obtained directly, as \hat{F}_{ix} cannot be calculated accurately based on a tire model. An estimation of the TRFC should be used in the

diagnosis design as well as in the faulty motor control gain estimation. As the models have been assumed to be precise, based on Eq. (14) one has the following holds after $\hat{\omega}_i$ and $\hat{\dot{\omega}}_i$ converge to 0

$$\phi_i(\hat{\mu}_i) = (k_i - k_{0i})u_i + (\hat{F}_{ix}(\hat{\mu}_i) - F_{ix})R_{\text{eff}} \quad (20)$$

where $\hat{\mu}_i$ is the estimated TRFC. As the $\hat{\mu}_i$ in the tire model is being updated, ϕ_i also changes accordingly. By assuming that the derivative of u_i , and thus that of F_{ix} , are ignorable and k_i is a piece-wise constant during the fault diagnosis process, the following holds:

$$\dot{\phi}_i \approx R_{\text{eff}} \frac{d\hat{F}_{ix}(\hat{\mu}_i)}{d\hat{\mu}_i} \frac{d\hat{\mu}_i}{dt} \quad (21)$$

Considering the following Lyapunov function candidate

$$V = \frac{1}{2} \phi_i^2(\hat{\mu}_i) \quad (22)$$

The time derivation of V is

$$\dot{V} = \phi_i(\hat{\mu}_i) \dot{\phi}_i(\hat{\mu}_i) \quad (23)$$

So the update law

$$\dot{\hat{\mu}}_i(t) = -L\phi_i(\hat{\mu}_i) \quad (24)$$

with $L > 0$ can make

$$\dot{\phi}_i = R_{\text{eff}} \dot{\hat{F}}_{ix}(\hat{\mu}_i) = R_{\text{eff}} \frac{d\hat{F}_{ix}(\hat{\mu}_i)}{d\hat{\mu}_i} \frac{d\hat{\mu}_i}{dt} = -R_{\text{eff}} \frac{d\hat{F}_{ix}(\hat{\mu}_i)}{d\hat{\mu}_i} L\phi_i(\hat{\mu}_i) \quad (25)$$

It is known that at a given tire slip angle α_i and a longitudinal slip ratio s_i , the tire longitudinal force F_{ix} increases with the increase of the TRFC, that is $\frac{dF_{ix}}{d\mu_i} > 0$, so the following will hold

$$\dot{V} = \hat{\phi}_i \dot{\phi}_i = -R_{\text{eff}} \frac{d\hat{F}_{ix}(\hat{\mu}_i)}{d\hat{\mu}_i} L\phi_i^2 < 0 \quad (26)$$

which means that the update law Eq. (24) can make ϕ_i converge to 0. Based on Eq. (20), one can see when both the motor and motor driver as a pair is working properly, $\phi_i \rightarrow 0$ will lead to $\hat{F}_{ix} \rightarrow F_{ix}$, which means $\hat{\mu}_i \rightarrow \mu_i$. However, if $k_i \neq k_{0i}$ due to a fault on a set of in-wheel motor/motor controller, after ϕ_i converges to 0, based on Eq. (20) one can have

$$\hat{F}_{ix}(\hat{\mu}_i) = \frac{(k_{0i} - k_i)u_i}{R_{\text{eff}}} + F_{ix}(\mu_i) \quad (27)$$

which means that $\hat{\mu}_i \neq \mu_i$. As the tire force model is assumed to be accurate, the estimated TRFCs based on the three healthy in-wheel motor/motor driver sets will be the same. It can be concluded that the motor/motor driver is in fault if the respective $\hat{\mu}_i$ is different from other three, with the assumption that only one of the four in-wheel motor/motor driver sets can be in fault.

3.2 Fault Diagnosis Design Considering Modeling Errors. The preceding fault diagnosis design was based on the assumption that the tire model, rolling resistance model, and all of the measured signals are accurate. However, this assumption will rarely hold due to modeling errors. Also it is challenging to obtain an accurate estimation of TRFC, especially at small slip regions [19–22]. In the presence of modeling errors, the tire force based on the tire model can be written as

$$\hat{F}_{ix}(\hat{\mu}_i, s_i) = \hat{F}_{0ix}(\hat{\mu}_i, s_i) + \Delta\hat{F}_{ix}(\hat{\mu}_i, s_i) \quad (28)$$

where s_i is the tire longitudinal slip. $\hat{F}_{0ix}(\hat{\mu}_i, s_i)$ is the accurate part of the tire model, i.e., $\hat{F}_{0ix}(\mu_i, s_i) = F_{ix}$, $\Delta\hat{F}_{ix}(\hat{\mu}_i, s_i)$ describes the tire force modeling error. Also assume the tire force model $\hat{F}_{ix}(\hat{\mu}_i, s_i)$ still satisfies $\frac{d\hat{F}_{ix}}{d\hat{\mu}_i} > 0$. Similar to the modeling-error-free case, the update law $\dot{\hat{\mu}}_i(t) = -L\phi_i$ can still make ϕ_i converges to 0. After $\hat{\omega}_i$, $\hat{\dot{\omega}}_i$, and ϕ_i converge, based on Eqs. (14) and (28), one has

$$(k_i - k_{0i})u_i + (\hat{F}_{0ix} - F_{ix} + d_i)R_{\text{eff}} = 0 \quad (29)$$

with

$$d_i = \Delta\hat{F}_{ix} + (\hat{F}_{i\text{-roll}} - F_{i\text{-roll}}) \quad (30)$$

Assume d_i is bounded as $|d_i| \leq d_0$. If there is no fault on the in-wheel motor/motor controller set, $k_i = k_{0i}$, $|\hat{F}_{0ix} - F_{ix}|$ will be finally bounded as

$$|\hat{F}_{0ix}(\hat{\mu}_i) - F_{ix}| \leq d_0 \quad (31)$$

However, if a fault occurs, $k_i \neq k_{0i}$, $|\hat{F}_{0ix} - F_{ix}|$ will satisfy

$$|\hat{F}_{0ix} - F_{ix}| = \left| \frac{(k_i - k_{0i})u_i}{R_{\text{eff}}} + d_i \right| \geq \left| \frac{(k_i - k_{0i})u_i}{R_{\text{eff}}} \right| - d_0 \quad (32)$$

which means that if the fault is sufficiently large, i.e., $|k_i - k_{0i}|$ is sufficiently large, the estimated TRFC will sufficiently differ from the other three TRFC estimations which are closely around the true value.

When $\phi_i = 0$ is satisfied, we have four estimated TRFCs, one for each wheel. As discussed above, the estimated TRFC based on the faulty wheel could be far away from the actual value, and the TRFC estimations based on other healthy wheels should be used to improve the accuracy of the control gain estimations. Thus, the control gain of each in-wheel motor/motor driver set can be calculated as

$$\hat{k}_i = \frac{I_\omega \hat{\dot{\omega}}_i + R_{\text{eff}}(\hat{F}_{ix}(\bar{\mu}) + \hat{F}_{i\text{-roll}})}{u_i} \quad (33)$$

where \hat{k}_i is the control gain estimation and $\bar{\mu}$ is the TRFC based on the three TRFC estimations whose values are most close to each other. As the longitudinal force curves of different TRFCs versus slip become very close to each other at small slip ratios (shown in Fig. 2), the TRFC estimation error could be very large at small slip region. Thus, among the three TRFC estimations which are most close to each other, the TRFC from the wheel with the largest slip is taken as $\bar{\mu}$. Note that the $|\hat{F}_{0ix}(\bar{\mu}) - F_{ix}| \leq |\hat{F}_{0ix}(\hat{\mu}_i) - F_{ix}|$ holds because $\bar{\mu}$ is closer to the actual TRFC than the $\hat{\mu}_i$.

Define the normalized error between \hat{k}_i and k_{0i} as

$$e_{ki} = \frac{\hat{k}_i - k_{0i}}{k_{0i}} \quad (34)$$

As the estimated wheel angular acceleration will converge to $\dot{\omega}_i$, based on Eqs. (11) and (33), one can have

$$\begin{aligned} e_{ki} &= \frac{I_\omega \dot{\omega}_i + R_{\text{eff}}(\hat{F}_{ix}(\bar{\mu}) + \hat{F}_{i\text{-roll}})}{u_i k_{0i}} - \frac{I_\omega \dot{\omega}_i + R_{\text{eff}}(F_{ix} + F_{i\text{-roll}})}{u_i k_{0i}} \\ &= \frac{R_{\text{eff}}(\hat{F}_{0ix}(\bar{\mu}) - F_{ix} + d_i)}{u_i k_{0i}} \end{aligned} \quad (35)$$

If $k_i = k_{0i}$ one has

$$|e_{ki}| = \left| \frac{R_{\text{eff}}(\hat{F}_{0ix}(\bar{\mu}) - F_{ix} + d_i)}{T_{0i}} \right| \leq \frac{2R_{\text{eff}}d_0}{T_{0i}} \quad (36)$$

However, if there is a fault happens, $k_i \neq k_{0i}$. e_{ki} can be written based on Eq. (29) as

$$\begin{aligned} e_{ki} &= \frac{\hat{k}_i - k_{0i}}{k_{0i}} = \frac{(\hat{k}_i - k_i) + (k_i - k_{0i})}{k_{0i}} \\ &= \left(\frac{I_\omega \dot{\omega}_i + R_{\text{eff}}(\hat{F}_{ix} + \hat{F}_{i\text{-roll}})}{T_{0i}} - \frac{I_\omega \dot{\omega}_i + R_{\text{eff}}(F_{ix} + F_{i\text{-roll}})}{T_{0i}} \right) \\ &\quad + \frac{k_i - k_{0i}}{k_{0i}} = \frac{R_{\text{eff}}(\hat{F}_{0ix} - F_{ix} + d_i)}{T_{0i}} + \frac{k_i - k_{0i}}{k_{0i}} \end{aligned} \quad (37)$$

So control gain estimation error e_{ki} and actual control gain k_i should satisfy

$$\left| e_{ki} - \frac{k_i - k_{0i}}{k_{0i}} \right| = \left| \frac{R_{\text{eff}}(\hat{F}_{0ix} - F_{ix} + d_i)}{T_{0i}} \right| \leq \frac{2R_{\text{eff}}d_0}{T_{0i}} \quad (38)$$

From Eqs. (36) and (38), it can be seen that when there is no fault, $k_i = k_{0i}$, the normalized error of control gain estimation e_{ki} should satisfy $|e_{ki}| \leq \frac{2R_{\text{eff}}d_0}{T_{0i}}$. $|e_{ki}| > \frac{2R_{\text{eff}}d_0}{T_{0i}}$ means a fault on motor/motor driver occurred. However, such a threshold value cannot detect all of the motor/motor controller faults. Based on Eq. (37), $|e_{ki}| > \frac{2R_{\text{eff}}d_0}{T_{0i}}$ can be triggered if

$$\begin{aligned} \left| \frac{k_i - k_{0i}}{k_{0i}} \right| &= \left| e_{ki} - \frac{R_{\text{eff}}(\hat{F}_{0ix} - F_{ix} + d_i)}{T_{0i}} \right| > \frac{2R_{\text{eff}}d_0}{T_{0i}} + \frac{2R_{\text{eff}}d_0}{T_{0i}} \\ &= \frac{4R_{\text{eff}}d_0}{T_{0i}} \end{aligned} \quad (39)$$

It should be noted that, however, as long as $\left| \frac{k_i - k_{0i}}{k_{0i}} \right| \leq \frac{4R_{\text{eff}}d_0}{T_{0i}}$ is satisfied, $k_i \neq k_{0i}$ may not be detected by the aforementioned fault diagnosis method. Thus, to trigger a fault alarm, Eq. (39) should be satisfied, which means that the fault should be relatively large enough to be detected due to the modeling errors. The bounds in Eqs. (36) and (38) are not fixed and can vary according to the applied motor torque control signals. At large torque values where the tire slip ratios are also large, the threshold value is small, but the threshold value becomes large at small torque regions, and the two bounds will intersect to each other. In general, a large threshold value may lead to misdiagnosis. However, it is worth mentioning that the effects of misdiagnosis at small slip region on the vehicle dynamics are slight as the force provided by the corresponding wheel is also small. It should be noted that, in this paper, the tires and road surface conditions of all the four wheels are assumed to be uniform.

4 Fault-Tolerant Control System Design for 4WIA Electric Vehicles

The control design is divided into two parts. A high-level controller is designed to produce a generalized forces/moment required to track the desired vehicle motion. A control allocation scheme is used to distribute the generalized control among the four wheels. Due to possible unmodeled dynamics as well as disturbances, the controller needs to be robust to the plant uncertainties. A sliding mode controller is thus used to enhance control system robustness.

4.1 High-Level Controller Design. Rewrite the vehicle model as

$$\begin{cases} \dot{V}_x = V_y \Omega_z - \frac{C_a}{M} V_x^2 + B_{Y1} F_Y - \frac{I_\omega B_{X1}}{R_{\text{eff}}} \dot{\omega} - B_{X1} F_{\text{roll}} + v_1 \\ \dot{V}_y = -V_x \Omega_z + \frac{1}{M} F_Y + B_{Y2} F_Y - \frac{I_\omega B_{X2}}{R_{\text{eff}}} \dot{\omega} - B_{X2} F_{\text{roll}} + v_2 \\ \dot{\Omega}_z = B_{Y3} F_Y - \frac{I_\omega B_{X3}}{R_{\text{eff}}} \dot{\omega} - B_{X3} F_{\text{roll}} + v_3 \end{cases} \quad (40)$$

where $\dot{\omega} = [\dot{\omega}_{fl} \ \dot{\omega}_{fr} \ \dot{\omega}_{rl} \ \dot{\omega}_{rr}]^T$, $B_Y = [B_{Y1} \ B_{Y2} \ B_{Y3}]^T$, $B_X = [B_{X1} \ B_{X2} \ B_{X3}]^T$, and $F_{\text{roll}} = [F_{fl\text{-roll}} \ F_{fr\text{-roll}} \ F_{rl\text{-roll}} \ F_{rr\text{-roll}}]^T$. A SMC is designed to produce the virtual control signals v_1 , v_2 , and v_3 . Since the control inputs and the controlled variables are decoupled, the above system can be partitioned into three single-input-single-output systems. Define the sliding surface for each channel as

$$S_n = x_n - x_{nr} \quad (41)$$

where x_{nr} is the vehicle state reference. Choose the Lyapunov functions for the three channels as

$$V_n = \frac{1}{2} S_n^2 \quad (42)$$

For channel 1, the time derivative of the above Lyapunov function is

$$\begin{aligned} \dot{V}_1 &= S_1 \dot{S}_1 = S_1 (\dot{x}_1 - \dot{x}_{1r}) \\ &= S_1 \left(V_y \Omega_z - \frac{C_a}{M} V_x^2 + B_{Y1} F_Y - \frac{I_\omega B_{X1}}{R_{\text{eff}}} \dot{\omega} - B_{X1} F_{\text{roll}} + v_1 - \dot{x}_{1r} \right) \end{aligned} \quad (43)$$

Choose the control law as

$$\begin{aligned} v_1 &= -V_y \Omega_z + \frac{C_a}{M} V_x^2 - B_{Y1} \hat{F}_Y + \frac{I_\omega B_{X1}}{R_{\text{eff}}} \dot{\omega} + B_{X1} \hat{F}_{\text{roll}} + \dot{x}_{1r} \\ &\quad - K_1 \text{sgn}(S_1) \end{aligned} \quad (44)$$

where K_1 is a positive constant, \hat{F}_Y and \hat{F}_{roll} are the estimated tire lateral force and rolling resistance vectors based on the measured signals including tire slip angles. When the tires experience both longitudinal slip and lateral slip angle, \hat{F}_Y should be estimated conservatively. It can be shown that the control law with K_1 being sufficiently large to over-power the uncertainties can make \dot{V}_1 negative definite. In order to avoid the chatting effect caused by the sign function, the sign function is replaced by a saturation function whose thickness is Φ_1 as

$$\text{sgn}(S_1) = \text{sgn} \left(\frac{S_1}{\Phi_1} \right) \quad (45)$$

Following the similar steps, the control laws for the other two surfaces can be obtained.

4.2 Control Allocation Design. A control allocation module is utilized to generate the four control signals in U for minimizing the cost function defined as

$$J = (v - BU)^T Q (v - BU) + b \|U\|^2 \quad (46)$$

where $Q = \text{diag}(q_1 \ q_2 \ q_3)$, b is a small positive constant, and the control signals in U are subject to their constraints. A numerical quadratic programming method can be used to solve this constrained optimization problem. The entries of the control effectiveness matrix B are pertinent to the four motor control gains k_i .

Table 1 Parameters of the vehicle model in CarSim

Parameters	Values
Sprung mass	600 kg
Total mass of in-wheel motor, wheel, and tire	45 kg
I_{ω}	3 kg m ²
R_{eff}	0.33 m
l_s	0.7 m
l_f	0.8 m
l_r	0.8 m

Details on control allocation methods are available in the literature such as Refs. [23–26]. When a fault on the in-wheel motor/motor driver is detected, the respective motor control gain will be reduced. The control effectiveness matrix B can be updated by using the estimated motor control gain by the method presented in Sec. 4.1 accordingly. The control allocation will then automatically distribute more torque among the remaining healthy motors to maintain the overall control objective. The lower bound $u_{i\text{min}}$ for the each of the control signals is 0. The upper bound $u_{i\text{max}}$ is the largest control signal that the motor driver allows.

5 Simulation Studies

Two simulations based on a high-fidelity full-vehicle model from CarSim® were conducted. In the first part of this section, the fault diagnosis results are presented, which is followed by the control results in the second part. The vehicle parameters in the simulations are listed in Table 1. These parameters are taken from an actual prototype 4WIA electric vehicle [27] in authors’ group at Ohio State University.

5.1 Fault Diagnosis Results

5.1.1 Diagnosis Without Considering Modeling Errors. If the tire model and TRFC are precisely known, the faulty wheel can be found by ϕ_i in the estimator, as the ϕ_i for the faulty wheel will not be 0. In this simulation the TRFC was set to 0.8, the desired torque of each motor was set to 90 Nm, and control gain of the rear-left wheel was reduced by 0.4 times after 3 s. The diagnosis result is shown in Fig. 3. As can be seen that ϕ_{rl} reduced from 0 to -36 Nm with other three ϕ_i still remaining at 0. Note that 36 Nm is exactly the torque the faulty wheel fails to give. It also shows that the faulty wheel control gain can be estimated with ϕ_i . Also note that in the simulation, the initial values for the ϕ_i were set nonzero.

If the TRFC is unknown, it can be estimated based on an accurate tire model. However, the estimated TRFC for the faulty wheel

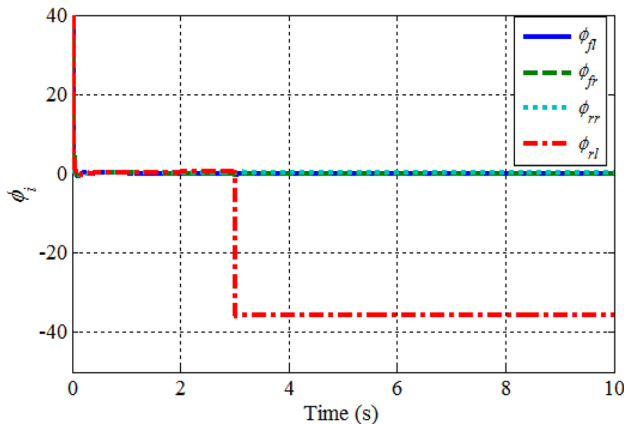


Fig. 3 Diagnosis results for accurate model and TRFC ($\mu = 0.8$, initial speed: 40 km/h)

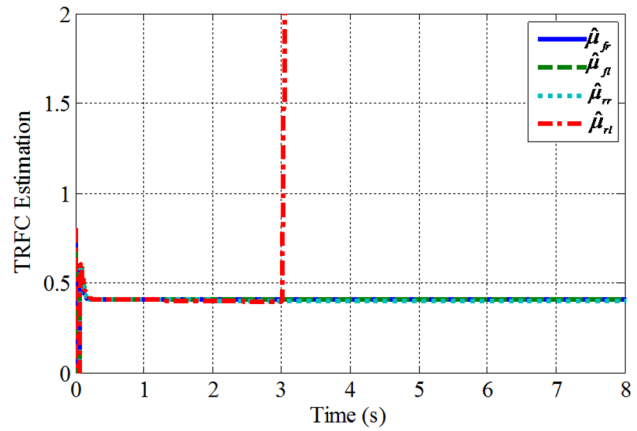


Fig. 4 Diagnosis result without modeling error ($\mu = 0.4$, initial speed: 15 km/h)

will be different from those of the other three. Figure 4 shows the simulation results when the TRFC is assumed to be unknown. The desired torque of each motor was also set to 90 Nm, and control gain of the faulty wheel was reduced after 3 s in the simulation. It can be observed that the estimated TRFCs are very accurate when the wheels are in healthy condition. The estimated TRFC based on the faulty wheel, as expected, is very different from the other three after 3 s. Note that the initial values for the estimated TRFCs were set as zero.

5.1.2 Fault Diagnosis Considering Modeling Errors. In this simulation, a modeling error was introduced by adding a bounded

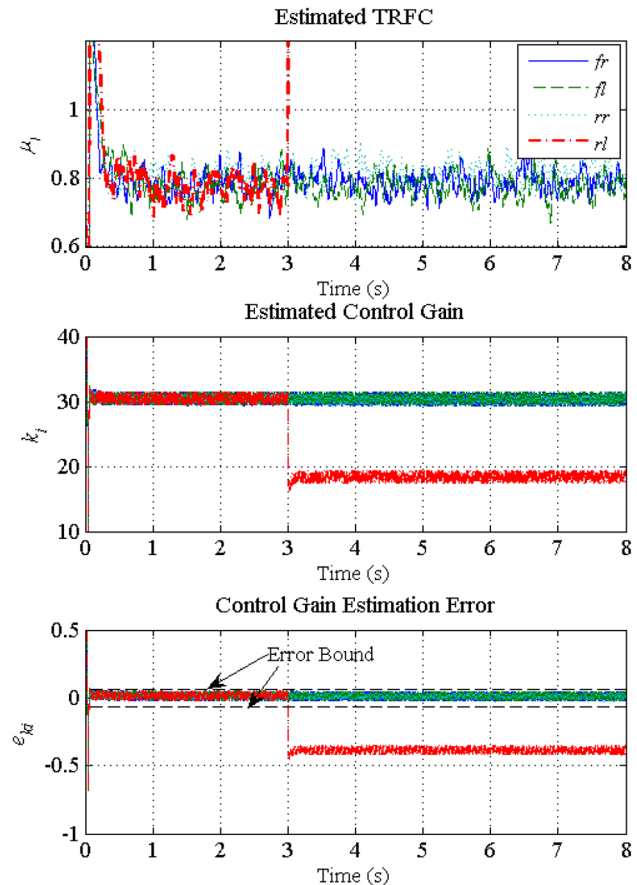


Fig. 5 TRFC and control gain estimations considering modeling error ($\mu = 0.8$, initial speed is 50 km/h)

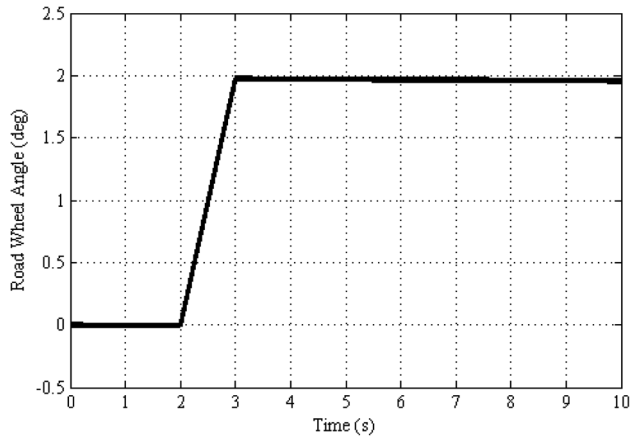


Fig. 6 Road wheel angle change of front wheels in the J-turn simulation

disturbance to the tire force. The simulation was carried out under the assumption that the real TRFC was 0.8, and the nominal control gain of the four in-wheels motors were 30. The fault was introduced by reducing the control gain of the rear-left motor to 0.6 times after 3 s. Figure 5 shows the estimation results for the four wheels. As it indicates, the TRFC estimations are less accurate due to the modeling error. However, the in-wheel motor control gain estimation errors are always bounded by Eq. (36) as long as the motor/motor driver sets are in good condition. It also can be seen that the control gain estimation for the faulty wheel was reduced to 0.6 times of its nominal value after 3 s. As the actual control gain of the faulty wheel was reduced by 0.4 times, the faulty wheel control gain estimation results matches the expectation well. The simulation illustrates that the fault diagnosis approach works well.

5.2 Fault-Tolerant Control Results. Three simulations were conducted in this section. In the first two parts of this section, the control results in a J-turn and a single-lane change are presented, respectively, to show the effectiveness of the proposed control method. The last simulation considers driver corrective steering action when a fault occurs, and the simulation results indicate that, due to the possible driver response lag, the proposed

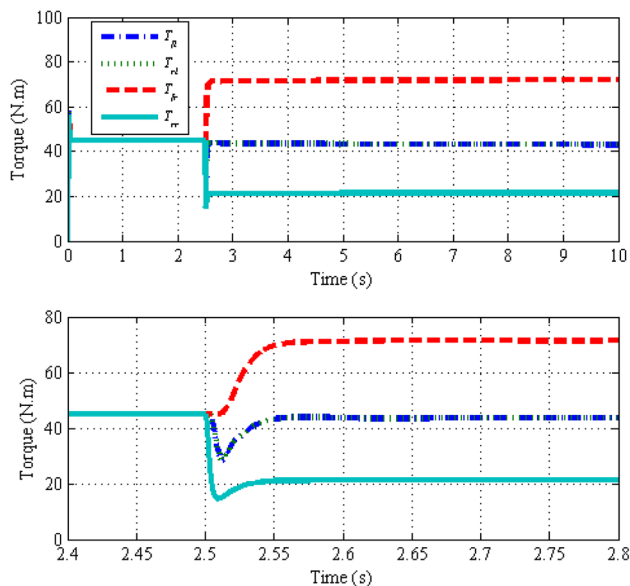


Fig. 7 Actual torques provided by the four motors, bottom figure shows the zoom-in

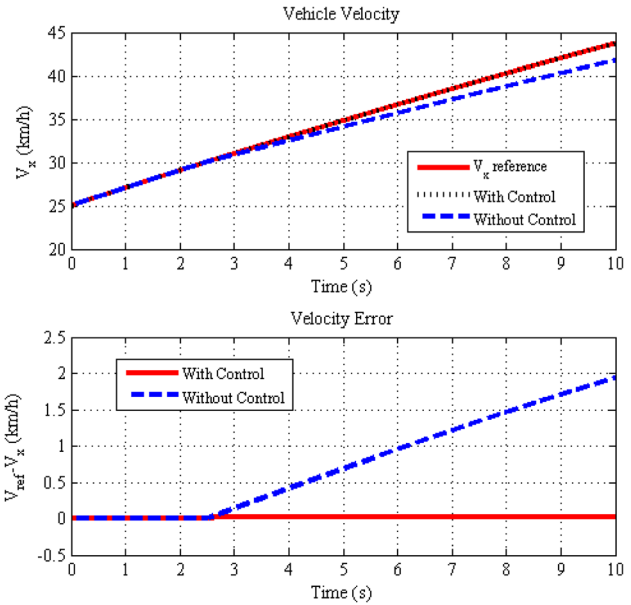


Fig. 8 Longitudinal velocity in the J-turn simulation

FTC is still necessary in maintaining the vehicle motion even if the driver can give good corrective steering action.

5.2.1 J-Turn During Acceleration. In the J-turn simulation, the TRFC was set to 0.8, and the initial vehicle speed was chosen as 25 km/h. The desired vehicle speed was accelerated to 44 km/h in 10 s. A counter-clockwise turn was introduced, and the change of road wheel angle of front wheels is shown in Fig. 6. At 2.3 s, a fault was added to the rear-right motor which made the control gain decrease to 0.3 times of its nominal value by multiplying the desired torque by 0.3. In the simulation, the estimated control gain of the faulty wheel was used in the controller as soon as a fault was detected. Simulation results are shown in Figs. 6–11. To more clearly illustrate the effectiveness of the proposed controller, the performance of an uncontrolled vehicle with the same fault and front wheels' road wheel angle was also plotted.

As shown in Fig. 7, the control allocation scheme dictated more desired torque to the healthy wheel on the same side of the faulty one to compensate its effect on the vehicle motion. It can be seen

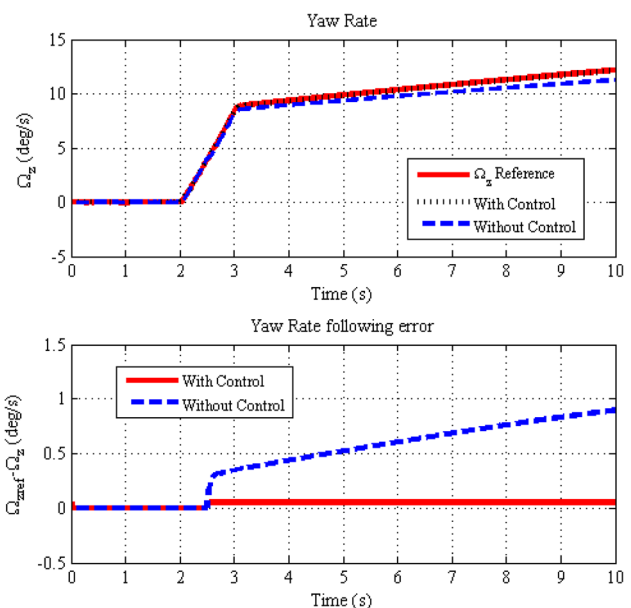


Fig. 9 Vehicle yaw rate change in the J-turn simulation

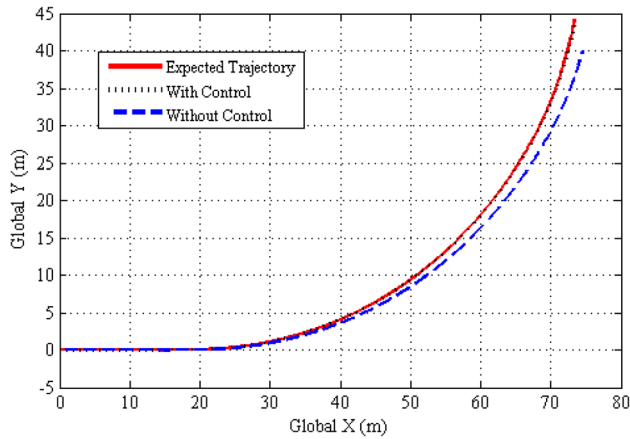


Fig. 10 Vehicle trajectory in the J-turn simulation

from Fig. 8 that the controlled vehicle can follow the reference velocity well, while the uncontrolled velocity failed to follow the reference velocity as the faulty wheel of the vehicle did not provide the desired torque and the lost torque was not allocated to other wheels. Similarly for the vehicle yaw rate, as can be seen in Fig. 9, the controlled vehicle can follow the yaw rate reference much better in comparison to the uncontrolled vehicle. The vehicle trajectory is shown in Fig. 10, it can be seen that the controlled vehicle can follow the expected trajectory, while the vehicle without control started deviating from the reference as soon as the fault was introduced.

5.2.2 Single-Lane Change During Acceleration. The J-turn simulation was conducted at low speed and high TRFC value. In the single-lane simulation, the initial speed was chosen as 80 km/h and the TRFC was set to 0.5. The front wheels' road wheel angle change is shown in Fig. 11. At the 2.3 s, a fault which made the rear-right motor control gain decrease to 0 was injected. The allocated desired torques for the four wheels are plotted in Fig. 12. Again, the control allocation scheme automatically distribute the torque requests among the healthy and faulty wheels to achieve the vehicle motion tracking control objectives even a fault occurred in one of the wheels. The vehicle longitudinal velocity, yaw rate, and lateral velocity results are shown in Figs. 13–15, respectively. The vehicle trajectory is shown in Fig. 16. It can be seen again that the proposed controller works well.

5.2.3 Acceleration Along a Straight Line. In the above simulations, the faulty vehicle driver's steering angles were the same as that of the healthy vehicle. In practical, however, the driver

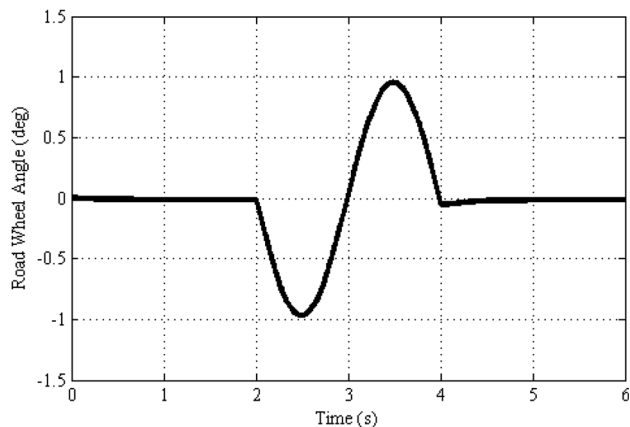


Fig. 11 Road wheel angle change of front wheels in the single-lane change simulation

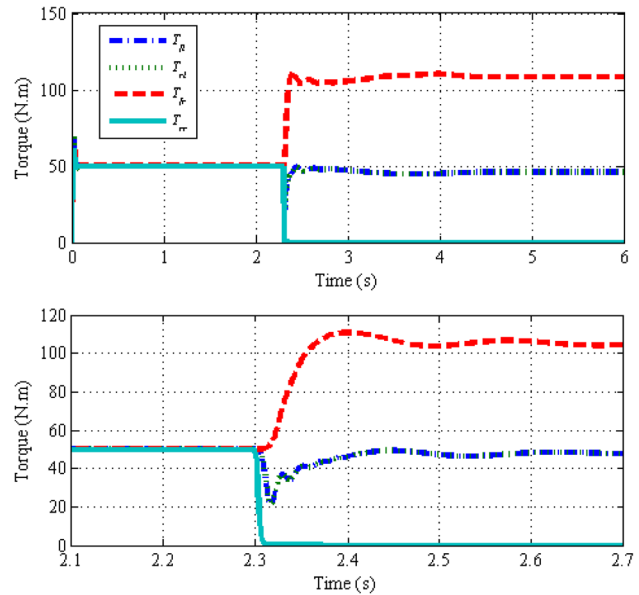


Fig. 12 Actual torques provided by the four motors, bottom figure shows the zoom-in

may provide a corrective steering angle to maintain the expected trajectory when the vehicle is found to deviate from the target trajectory. In this simulation, the driver corrective steering is considered. A driver-vehicle model [28] is used to simulate the driver behavior and generate the corrective steering action. Due to the typical driver's response lag between the time the driver takes action and the vehicle starts deviating from the expected trajectory, the driver's corrective steering angle can be written as

$$\sigma_c = \begin{cases} 0 & \text{if } (t - t_f \leq \tau_3) \\ \frac{h\varepsilon}{1 + \tau_1 s} e^{-\tau_2 s} & \text{if } (t - t_f > \tau_3) \end{cases} \quad (47)$$

where σ_c is the driver's corrective steering angle which will correct the vehicle motion after the driver realizes the vehicle is deviating

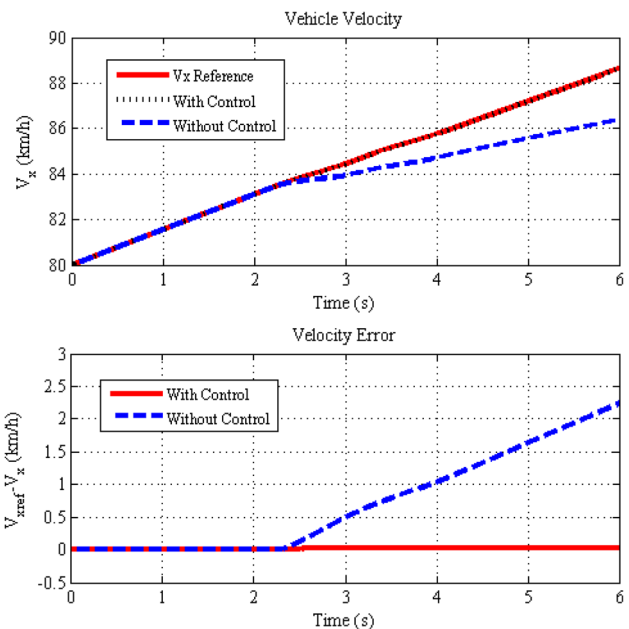


Fig. 13 Longitudinal velocity in the single-lane change simulation

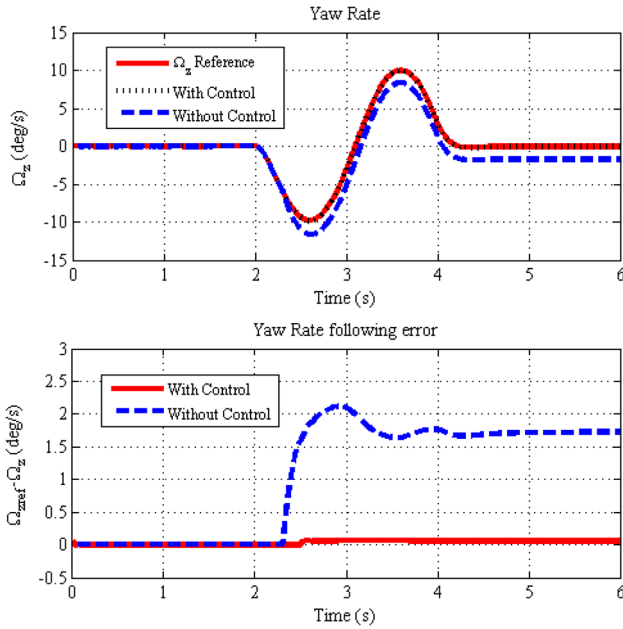


Fig. 14 Yaw rate in the single-lane change simulation

from the expected trajectory, t_f is the time a fault occurs, τ_3 is driver's response lag between the driver starts to take action and t_f , ε is the error between the target path and the actual vehicle position, please refer to Ref. [27] for the calculation of ε in detail. τ_1 and τ_2 are constant values and are used to describe the driver's steering nature. We assume that the driver will give fast and precise corrective steering as soon as the he/she notices the vehicle is deviating from the reference, so both of τ_1 and τ_2 are chosen to be small (0.02 s in this study). Note that choosing large values τ_1 and τ_2 will induce bad corrective steering as large τ_1 and τ_2 mean slow and imprecise steering. Only the response lag τ_3 is studied.

In this simulation, the vehicle was expected to run in a straight line and the speed was to be accelerated from 90 km/h to 103 km/h in 10 s. The TRFC is set to 0.8. At 2 s, when the vehicle was at 50 m from the starting point, a fault which made the rear-right motor control gain decrease to zero was injected. The effects

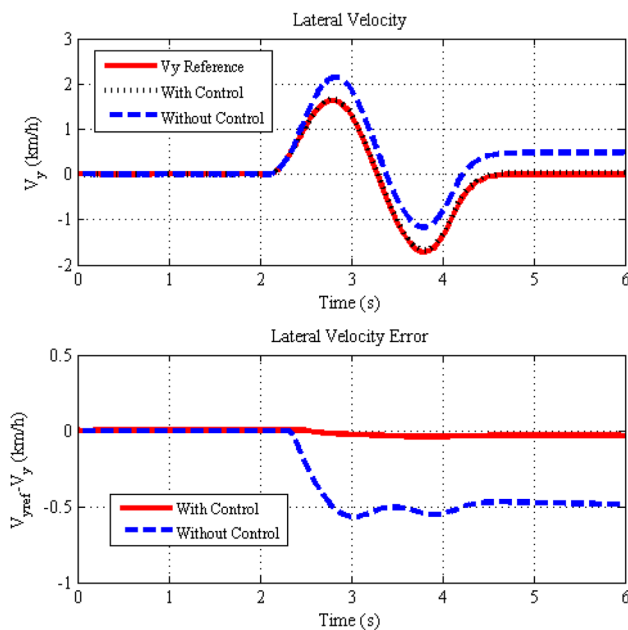


Fig. 15 Lateral velocity in the single-lane change simulation

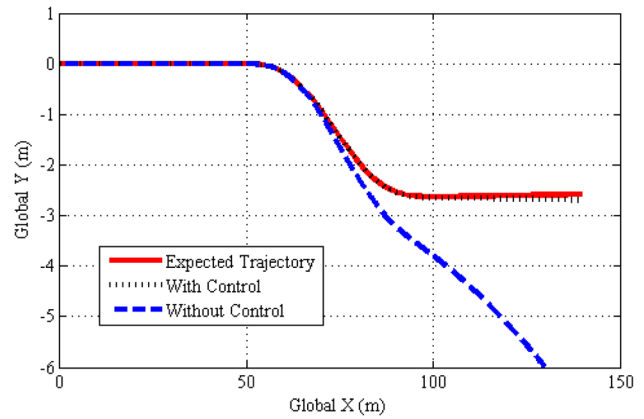


Fig. 16 Vehicle trajectory in the single-lane change simulation

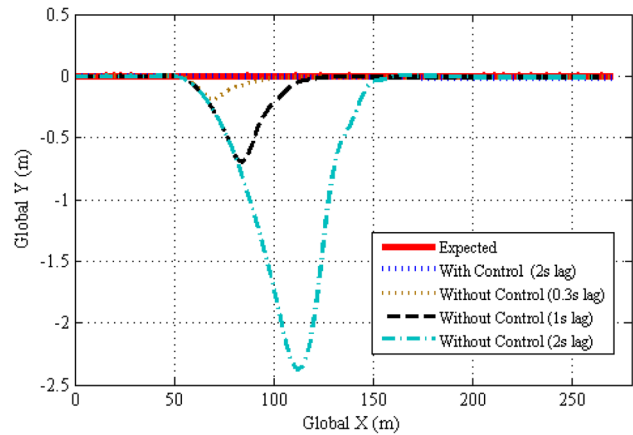


Fig. 17 Vehicle trajectory in a straight line acceleration case

of different response lags to the vehicle motions are investigated and the vehicle trajectories are shown in Fig. 17. It can be seen that the vehicle trajectory can be corrected fast by the corrective steering action and no overshooting in the vehicle lateral motion is observed. So the corrective steering works well as soon as the driver takes action. However, it can also be found that the response lag affects the vehicle lateral motion considerably. For example, a 2 s response lag will induce 2.3 m error in the lateral position, and 1 s response lag will still cause 0.7 m error. Such big unexpected lateral motions may increase the chance of accident when the vehicle running at high speed. Note that the controlled vehicle can always follow the target trajectory even if the driver's response lag is large (2 s). Also note that this simulation is performed under the assumption that the driver can give very good corrective steering action as long as he/she observes the vehicle starts to deviate. In practical, however, as the vehicle yaw rate will change fast when a fault occurs, the driver may become panic and give wrong corrective steering action, which may induce accidents.

6 Conclusions

An in-wheel motor/motor driver fault diagnosis approach for a 4WIA electric vehicle is proposed. The proposed diagnosis approach does not need an accurate TRFC knowledge and can estimate the control gains of the four motors accurately. It is also shown that the diagnosis approach can work well in the existence of tire force modeling error. Based on the in-wheel motor/motor driver fault detection mechanism, a control-allocation based vehicle control system is designed to accommodate the in-wheel motor/motor driver fault by automatically allocating the control effort among other healthy wheels. Simulations using

a high-fidelity CarSim® full-vehicle model show the effectiveness of the proposed in-wheel motor fault diagnosis and fault-tolerant control approaches in different driving scenarios.

Nomenclature

V_x = vehicle longitudinal speed at center of gravity
 V_i = traveling velocity at the center of the i th wheel
 V_y = vehicle lateral speed
 Ω_z = vehicle yaw rate
 M = mass of the vehicle
 I_z = yaw inertia of the vehicle
 I_ω = wheel rotational inertia
 e_{ki} = control gain estimation error of each pair of the in-wheel motor and driver
 d_0 = disturbance bound
 F_z = tire normal load
 C_a = aerodynamic drag coefficient
 s_i = slip ratio of the i th wheel
 F_x = effective longitudinal force acting on vehicle C.G.
 F_y = effective lateral force acting on vehicle C.G.
 F_{i_roll} = tire rolling resistance of the i th in-wheel motor
 \hat{F}_{i_roll} = tire rolling resistance of the i th in-wheel motor based on rolling resistance model
 M_z = effective yaw-moment acting on vehicle C.G.
 μ = frictional coefficient
 $\hat{\mu}_i$ = estimation of frictional coefficient based on the i th wheel
 u_i = control input to the i th in-wheel motor driver
 ω_i = wheel rotational speed of the i th wheel
 α_i = slip angle of the i th wheel
 R_{eff} = tire effective rolling radius in meter
 k_{0i} = nominal control gain of the i th motor/motor driver
 k_i = actual control gain of the i th motor/motor driver
 \hat{k}_{i_est} = estimation of control gain for the i th motor/motor driver
 T_i = torque provided by the i th in-wheel motor
 σ = road wheel angle of front wheels
 σ_c = driver's corrective steering angle after a fault occurs

References

- [1] Chan, C. C., 2002, "The State of the Art of Electric and Hybrid Vehicles," *Proc. IEEE*, **90**, pp. 247–275.
- [2] Delucchi, M. A., and Lipman, T. E., 2001, "An Analysis of the Retail and Lifecycle Cost of Battery-Powered Electric Vehicles," *Transp. Res. D*, **6**(6), pp. 371–404.
- [3] Yamakawa, J., Kojima, A., and Watanabe, K., 2007, "A Method of Torque Control for Independent Wheel Drive Vehicles on Rough Terrain," *J. Terramech.*, **44**(5), pp. 371–381.
- [4] Shino, M., and Nagai, M., 2003, "Independent Wheel Torque Control of Small-Scale Electric Vehicle for Handling and Stability Improvement," *JSAE Rev.*, **24**(4), pp. 449–456.
- [5] Piyabongkarn, D., Rajamani, R., and Lew, J. Y., 2010, "Active Driveline Torque Management Systems—Individual Wheel Torque Control for Active Automotive Safety Applications," *IEEE Control Syst. Mag.*, **30**(4), pp. 86–102.

- [6] Peng, H., and Tomizuka, M., 1993, "Preview Control for Vehicle Lateral Guidance in Highway Automation," *J. Dyn. Syst., Meas., Control*, **115**(5), pp. 679–686.
- [7] Wang, J., and Hsieh, M. F., 2009, "Vehicle Yaw-Inertia- and Mass-Independent Adaptive Steering Control," *Proc. Inst. Mech. Eng., Part D (J. Automob. Eng.)*, **223**(9), pp. 1101–1108.
- [8] Liang, W., Yu, H., McGee, R., Kuang, M., and Medanic, J., 2009, "Vehicle Pure Yaw-Moment Control Using Differential Tire Slip," *American Control Conference*, June 10–12, pp. 3331–3336.
- [9] Chamseddine, A., and Noura, H., 2008, "Control and Sensor Fault Tolerance of Vehicle Active Suspension," *IEEE Trans. Control Syst. Technol.*, **16**(3), pp. 416–433.
- [10] Jayabalan, R., and Fahimi, B., 2006, "Monitoring and Fault Diagnosis of Multi-converter Systems in Hybrid Electric Vehicles," *IEEE Trans. Veh. Technol.*, **55**(5), pp. 1475–1484.
- [11] Oudghiri, M., Chadli, M., Hajjaji, A., 2008, "Robust Observer-based Fault-tolerant Control for Vehicle Lateral Dynamics," *Int. J. Veh. Des.*, **48**(3/4), pp. 173–189.
- [12] Wallmark, O., Harnefors, L., and Carlson, O., 2007, "Control Algorithms for a Fault-Tolerant PMSM Drive," *IEEE Trans. Ind. Electron. Control Instrum.*, **54**(4), pp. 1973–1980.
- [13] Muenchhof, M., Beck, M., and Isermann, R., 2009, "Fault-tolerant Actuators and Drives—Structures, Fault Detection Principles and Applications," *Annu. Rev. Control*, **33**(2), pp. 136–148.
- [14] Wong, J. W., 2001, *Theory of Ground Vehicles*, 3rd ed., Wiley, New York.
- [15] Wang, J., and Longoria, R. G., 2009, "Coordinated and Reconfigurable Vehicle Dynamics Control," *IEEE Trans. Control Syst. Technol.*, **17**(3), pp. 723–732.
- [16] Di Cairano, S., and Tseng, H. E., 2010, "Driver-assist Steering by Active Front Steering and Differential Braking: Design, Implementation and Experimental Evaluation of a Switched Model Predictive Control Approach," *Proceedings of the 49th IEEE Conference on Decision and Control*, Dec. 2010, pp. 2886–2891.
- [17] Pacejka, H. B., and Bakker, E., 1993, "Magic Formula Tire Model," *Veh. Syst. Dyn.*, **21**, pp. 1–18.
- [18] Rajamani, R., Piyabongkarn, D., Lew, J. Y., and Grogg, J. A., 2006, "Algorithms for Real-Time Estimation of Individual Wheel Tire-Road Friction Coefficients," *Proceedings of the American Control Conference*, pp. 4682–4687.
- [19] Li, L., Wang, F. Y., and Zhou, Q., 2006, "Integrated Longitudinal and Lateral Tire/road Friction Modeling and Monitoring for Vehicle Motion Control," *IEEE Trans. Intell. Transp. Syst.*, **7**(1), pp. 1–19.
- [20] Gustafsson, F., 1997, "Slip-Based Tire-Road Friction Estimation," *Automatica*, **33**(6), pp. 1087–1099.
- [21] Wang, J., Alexander, L., and Rajamani, R., 2004, "Friction Estimation on Highway Vehicles Using Longitudinal Measurements," *ASME J. Dyn. Syst., Meas. Control*, **126**(2), pp. 265–275.
- [22] Chen, Y., and Wang, J., 2011, "Adaptive Vehicle Speed Control with Input Injections for Longitudinal Motion Independent Road Frictional Condition Estimation," *IEEE Trans. Veh. Technol.*, **60**(3), pp. 839–848.
- [23] Plumlee, J. H., Bevely, D. M., and Hodel, A. S., 2004, "Control of a Ground Vehicle Using Quadratic Programming Based Control Allocation Techniques," *American Control Conference*, Boston, pp. 4704–4709.
- [24] Bodson, M., 2002, "Evaluation of Optimization Methods for Control Allocation," *J. Guid. Control Dyn.*, **25**(4), pp. 703–711.
- [25] Härkegård, O., and Glad, S., 2005, "Resolving Actuator Redundancy—Optimal Control Versus Control Allocation," *Automatica*, **41**(1), pp. 137–144.
- [26] Durham, W. C., 1993, "Constrained Control Allocation," *J. Guid. Control Dyn.*, **16**(4), pp. 717–725.
- [27] Wang, R., Chen, Y., Feng, D., Huang, X., and Wang, J., 2011, "Development and Performance Characterization of an Electric Ground Vehicle With Independently Actuated In-Wheel Motors," *J. Power Sources*, **196**(8), pp. 3962–3971.
- [28] Mokhiamar, O., and Abe, M., 2004, "Simultaneous Optimal Distribution of Lateral and Longitudinal Tire Forces for the Model Following Control," *J. Dyn. Syst., Meas., Control*, **126**(4), pp. 753–763.